J|A|C|S
ARTICLES
Published on Web 05/17/2007

VTVH-MCD and DFT Studies of Thiolate Bonding to $\{FeNO\}^7$/$\{FeO_2\}^8$ Complexes of Isopenicillin *N* Synthase: Substrate Determination of Oxidase versus Oxygenase Activity in Nonheme Fe Enzymes

Christina D. Brown,[†] Michael L. Neidig,[†] Matthew B. Neibergall,[‡] John D. Lipscomb,*[,‡] and Edward I. Solomon*[,†]

Contribution from the Department of Chemistry, Stanford University, Stanford, California 94305-5080, and Department of Biochemistry, Molecular Biology and Biophysics and the Center for Metals in Biocatalysis, University of Minnesota, Minneapolis, Minnesota 55455

Received February 26, 2007; E-mail: lipsc001@umn.edu; edward.solomon@stanford.edu

Abstract: Isopenicillin *N* synthase (IPNS) is a unique mononuclear nonheme Fe enzyme that catalyzes the four-electron oxidative double ring closure of its substrate ACV. A combination of spectroscopic techniques including EPR, absorbance, circular dichroism (CD), magnetic CD, and variable-temperature, variable-field MCD (VTVH-MCD) were used to evaluate the geometric and electronic structure of the $\{FeNO\}^7$ complex of IPNS coordinated with the ACV thiolate ligand. Density Function Theory (DFT) calculations correlated to the spectroscopic data were used to generate an experimentally calibrated bonding description of the Fe−IPNS−ACV−NO complex. New spectroscopic features introduced by the binding of the ACV thiolate at 13 100 and 19 800 cm^{-1} are assigned as the NO π^*(ip) → Fe $d_{x^2-y^2}$ and S π→ Fe $d_{x^2-y^2}$ charge transfer (CT) transitions, respectively. Configuration interaction mixes S CT character into the NO π^*(ip) → Fe $d_{x^2-y^2}$ CT transition, which is observed experimentally from the VTVH-MCD data from this transition. Calculations on the hypothetical $\{FeO_2\}^8$ complex of Fe−IPNS−ACV reveal that the configuration interaction present in the $\{FeNO\}^7$ complex results in an unoccupied frontier molecular orbital (FMO) with correct orientation and distal O character for H-atom abstraction from the ACV substrate. The energetics of NO/O_2 binding to Fe−IPNS−ACV were evaluated and demonstrate that charge donation from the ACV thiolate ligand renders the formation of the Fe^{III}-superoxide complex energetically favorable, driving the reaction at the Fe center. This single center reaction allows IPNS to avoid the O_2 bridged binding generally invoked in other nonheme Fe enzymes that leads to oxygen insertion (i.e., oxygenase function) and determines the oxidase activity of IPNS.

1. Introduction

Mononuclear nonheme iron enzymes catalyze a wide variety of medically, pharmaceutically, and biologically important reactions.[1,2] These enzymes can be divided into two groups, one which binds an organic substrate to an Fe^{III} center and activates it for reaction with triplet O_2 and the other which binds oxygen to an Fe^{II} center and activates it for reaction with an organic substrate.[3] The oxygen activating enzymes include the α-ketogulatare (αKG)-dependent dioxygenases, the pterin-dependent hydroxylases, the extradiol dioxygenases, and the Rieske dioxygenases. These enzymes share a common active site Fe-binding motif of two histidines and one carboxylate, known as the facial triad.[4] The majority of these enzymes also exhibit a common reactivity, acting as oxygenases that insert either one or two oxygen atoms from O_2 into the substrate or cofactor. However, two Fe^{II}/O_2 activating enzymes, Isopenicillin N-synthase (IPNS) and 1-aminocyclopropane-1-carboxylic acid oxidase (ACCO), have a high sequence homology to the αKG-dependent dioxygenases but exhibit very different reactivity from that of the oxygenases. Both IPNS and ACCO are oxidases that utilize O_2 for substrate oxidation, which is proposed to occur through an initial H-atom abstraction.[5−10]

Isopenicillin N-synthase is an enzyme found in fungi and bacteria that catalyzes the formation of isopenicillin N, a bicyclic precursor to the β lactam antibiotics including the penicillins and cephalosporins.[5−6] IPNS binds a tripeptide substrate δ-(L-α-aminoadipoyl)-L-cysteinyl-D-valine (ACV) and performs a

[†] Stanford University.
[‡] University of Minnesota.

(1) Feig, A. L.; Lippard, S. J. *Chem. Rev.* **1994**, *94*, 759−805.
(2) Que, L.; Ho, R. Y. N. *Chem. Rev.* **1996**, *96*, 2607−2624.
(3) Solomon, E. I.; Brunold, T. C.; Davis, M. I.; Kemsley, J. N.; Lee, S.-K.; Lehnert, N.; Neese, F.; Skulan, A. J.; Yang, Y.-S.; Zhou, J. *Chem. Rev.* **2000**, *100*, 235−349.
(4) Hegg, E. L.; Que, L., Jr. *Eur. J. Biochem.* **1997**, *250*, 625−629.
(5) Baldwin, J. E.; Adlington, R. M.; Moroney, S. E.; Field, L. D.; Ting, H. H. *J. Chem. Soc., Chem. Commun.* **1984**, 984−986.
(6) Baldwin, J. E.; Abraham, E. *Nat. Prod. Rep.* **1988**, *5*, 129−145.
(7) Baldwin, J. E.; Bradley, M. *Chem. Rev.* **1990**, *90*, 1079−1088.
(8) Rocklin, A. M.; Tierney, D. L.; Kofman, V.; Brunhuber, N. M. W.; Hoffman, B. M.; Christoffersen, R. E.; Reich, N. O.; Lipscomb, J. D.; Que, L., Jr. *Proc. Natl. Acad. Sci. U.S.A.* **1999**, *96*, 7905−7909.
(9) Zhou, J.; Rocklin, A. M.; Lipscomb, J. D.; Que, L., Jr.; Solomon, E. I. *J. Am. Chem. Soc.* **2002**, *124*, 4602−4609.
(10) Rocklin, A. M.; Kato, K.; Liu, H.-w.; Que, L.; Lipscomb, J. D. *J. Biol. Inorg. Chem.* **2004**, *9*, 171−182.

10.1021/ja071364v CCC: $37.00

Scheme 1. IPNS Catalyzes a Four-Electron Oxidative Double Ring Closure of ACV to Form Isopenicillin N

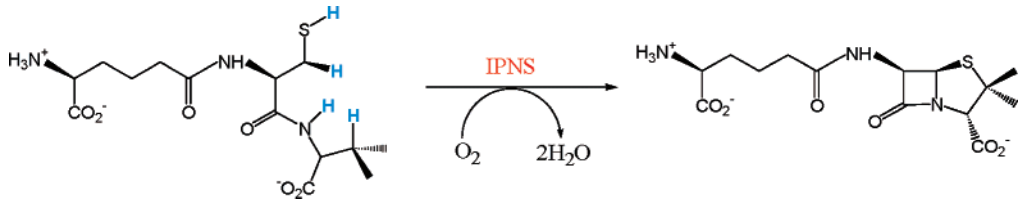

four-electron oxidative ring closure, fully reducing 1 equiv of O_2 to H_2O and closing the β lactam and thiazolidine rings of isopenicillin N (Scheme 1).[11−14] The crystal structure of the resting form of the enzyme complexed with Mn shows a six-coordinate metal site with two histidines, one aspartate, two waters, and a glutamine.[15] Upon substrate binding, the crystal structure of the Fe^{II}−IPNS−ACV complex shows that the glutamine is displaced by the cysteinyl S of ACV and one of the water molecules is lost, freeing a coordination position for O_2 binding.[16] From these crystal structures and ACV analogue studies, a reaction mechanism has been proposed for IPNS in which O_2 binds end-on to Fe^{II} and abstracts a methylene H from the cysteinyl β C in the first step.[5,7,17]

H-atom abstraction by metal-superoxide complexes has been invoked in the mechanisms of several metalloenzymes, including the noncoupled binuclear Cu enzyme peptidylglycine-hydroxylating monooxygenase (PHM)[18−20] and the binuclear Fe enzyme *myo*-inositol oxygenase (MIOX).[21] Experimentally, a Fe^{III}/Fe^{III}-superoxide intermediate of MIOX has been isolated and characterized by EPR. While the proposed IPNS−ACV reaction mechanism calls for H-atom abstraction by an FeO_2 complex, there is little evidence to support the formation of Fe^{III}-superoxide in the reactions of mononuclear nonheme Fe enzymes.

While mononuclear nonheme Fe enzymes are relatively inert to reaction with O_2 in the absence of substrate or cofactor, in most cases they react readily with NO to form stable $\{FeNO\}^7$ complexes both with and without substrates and cofactors.[3] In addition, the binding of NO creates an EPR active center, which is also chromophoric, allowing for the application of a variety of spectroscopic techniques.[22,23] $\{FeNO\}^7$ complexes of many mononuclear nonheme Fe enzymes have been prepared including those of phenylalanine hydroxylase,[24] the Rieske dioxygenases,[25] and IPNS.[11,17] The crystal structure of Fe−IPNS−ACV−NO shows a six-coordinate Fe center with NO occupying the coordination position opened by ACV binding to Fe.[17] Previous EPR and Mössbauer studies of Fe−IPNS−ACV−NO demonstrate that the complex has an $S = {}^3/_2$ ground state, which is mostly axial but becomes slightly rhombic upon ACV addition.[11] From absorbance studies, the addition of ACV to Fe−IPNS−NO introduces new features at 508 and 720 nm.[11] A DFT study of Fe−IPNS−ACV−NO calculates a shortened Fe−NO bond distance and larger Fe−N−O bond angle relative to the crystal structure.[26]

While many studies of $\{FeNO\}^7$ complexes of mononuclear nonheme enzymes provided valuable information on the structures of the active sites, the electronic structure of the $\{FeNO\}^7$ unit was not fully understood. Spectroscopic and DFT studies of $\{FeNO\}^7$ model complexes have elucidated the oxidation and spin states of both the Fe and NO moieties and their bonding interactions within the $\{FeNO\}^7$ unit.[27,28] The electronic structure of the $\{FeNO\}^7$ unit was shown to be best described as high-spin Fe^{III} ($S = {}^5/_2$) antiferromagnetically coupled to NO^- ($S = 1$) to give a total spin of $S = {}^3/_2$. Five key transitions in the absorbance/CD/MCD spectra of the model complexes were identified as two Fe d → d Ligand Field (LF) transitions and three NO $2\pi^*$ → Fe d Charge Transfer (CT) transitions. Different combinations of basis sets and functionals were used to optimize the $\{FeNO\}^7$ model complexes and were calibrated using experimental geometric and spectroscopic parameters for the complexes. Using this calibrated method, NO was replaced by O_2 in the model complex and the electronic structure of the hypothetical $\{FeO_2\}^8$ complex was described. The energetics of NO and O_2 binding to Fe^{II} model complexes were also calculated and found to be exergonic for NO and endergonic for O_2, the result of $Fe^{III}-NO^-$ forming a stronger bond than $Fe^{III}-O_2^{\bullet-}$.

In this study, we apply the spectroscopic and DFT methodology developed to study the $\{FeNO\}^7$ model complexes to the Fe−IPNS−ACV−NO enzyme complex. We use a combination of EPR, absorbance, CD, MCD, and VTVH-MCD spectroscopy to identify new spectral features introduced by the binding of the ACV thiolate to the IPNS $\{FeNO\}^7$ complex. From these new spectral features, we use DFT calculations to determine the effects of the ACV thiolate on the $Fe^{III}-NO^-$ bond. Extending our DFT study to the Fe−IPNS−ACV−O_2 complex,

(11) Chen, V.; Orville, A.; Harpel, M.; Frolik, C.; Surerus, K.; Munck, E.; Lipscomb, J. *J. Biol. Chem.* **1989**, *264*, 21677−21681.
(12) Orville, A. M.; Chen, V. J.; Kriauciunas, A.; Harpel, M. R.; Fox, B. G.; Munck, E.; Lipscomb, J. D. *Biochemistry* **1992**, *31*, 4602−4612.
(13) Randall, C. R.; Zang, Y.; True, A. E.; Que, L. ,Jr.; Charnock, J. M.; Garner, C. D.; Fujishima, Y.; Schofield, C. J.; Baldwin, J. E. *Biochemistry* **1993**, *32*, 6664−6673.
(14) Scott, R. A.; Wang, S.; Eidsness, M. K.; Kriauciunas, A.; Frolik, C. A.; Chen, V. J. *Biochemistry* **1992**, *31*, 4596−4601.
(15) Roach, P. L.; Clifton, I. J.; Fulop, V.; Harlos, K.; Barton, G. J.; Hajdu, J.; Andersson, I.; Schofield, C. J.; Baldwin, J. E. *Nature (London)* **1995**, *375*, 700−704.
(16) Roach, P. L.; Clifton, I. J.; Hensgens, C. M. H.; Shibata, N.; Long, A. J.; Strange, R. W.; Hasnain, S. S.; Schofield, C. J.; Baldwin, J. E.; Hajdu, J. *Eur. J. Biochem.* **1996**, *242*, 736−740.
(17) Roach, P. L.; Clifton, I. J.; Hensgens, C. M. H.; Shibta, N.; Schofield, C. J.; Hajdu, J.; Baldwin, J. E. *Nature (London)* **1997**, *387*, 827−830.
(18) Chen, P.; Solomon, E. I. *J. Am. Chem. Soc.* **2004**, *126*, 4991−5000.
(19) Prigge, S. T.; Eipper, B. A.; Mains, R. E.; Amzel, L. M. *Science* **2004**, *304*, 864−867.
(20) Francisco, W. A.; Blackburn, N. J.; Klinman, J. P. *Biochemistry* **2003**, *42*, 1813−1819.
(21) Xing, G.; Diao, Y.; Hoffart, L. M.; Barr, E. W.; Prabhu, K. S.; Arner, R. J.; Reddy, C. C.; Krebs, C.; Bollinger, J. M. Jr. *Proc. Natl. Acad. Sci. U.S.A.* **2006**, *103*, 6130−6135.
(22) Arciero, D.; Lipscomb, J.; Huynh, B.; Kent, T.; Munck, E. *J. Biol. Chem.* **1983**, *258*, 14981−14991.
(23) Westcott, B. L.; Enemark, J. H. Transition Metal Nitrosyls. In *Inorganic Electronic Structure and Spectroscopy, Volume II. Applications and Case Studies*; Solomon, E. I., Lever, A. B. P., Eds.; John Wiley and Sons: New York, 1999; pp 403−450.
(24) Han, A. Y.; Lee, A. Q.; Abu-Omar, M. M. *Inorg. Chem.* **2006**, *45*, 4277−4283.
(25) Yang, T. C.; Wolfe, M. D.; Neibergall, M. B.; Mekmouche, Y.; Lipscomb, J. D.; Hoffman, B. M. *J. Am. Chem. Soc.* **2003**, *125*, 7056−7066.
(26) Zhang, Y.; Oldfield, E. *J. Am. Chem. Soc.* **2004**, *126*, 9494−9495.
(27) Brown, C. A.; Pavlosky, M. A.; Westre, T. E.; Zhang, Y.; Hedman, B.; Hodgson, K. O.; Solomon, E. I. *J. Am. Chem. Soc.* **1995**, *117*, 715−732.
(28) Schenk, G.; Pau, M. Y. M.; Solomon, E. I. *J. Am. Chem. Soc.* **2004**, *126*, 505−515.

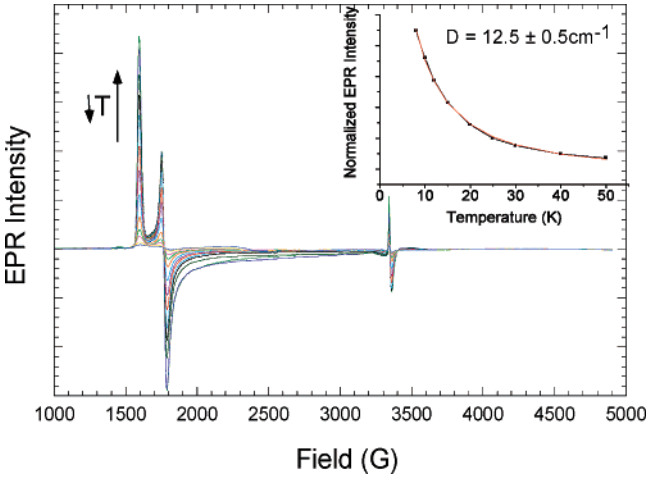

Figure 1. Temperature-dependent EPR spectra of Fe−IPNS−ACV−NO and Boltzmann fit to the Curie law of relative EPR intensities to give an axial ZFS value of $D = 12.5 \pm 0.5$ cm^{-1} (inset).

we evaluate how the features of the Fe^{III}−O$_2^{\bullet-}$ bond lead to the unique oxidase activity of IPNS.

2. Experimental Procedures

2.1. Materials. ACV was purchased from Bachem. The IPNS expression vector pIT353 was a gift from Victor Chen (Eli Lilly).[29] Cellufine A-800 anion exchange resin was purchased from Millipore and is now available from Chisso America Incorporated.

2.2. Sample Preparation. Isopenicillin *N*-synthase was overexpressed in *E. coli* K12 JM109 and purified from inclusion bodies in the apo form according to previously published procedures.[30] A small amount (~1 mg) of DNAse I was added to the buffer used to resuspend the cell pellet prior to sonication. Dissolution of the inclusion bodies in 7 M urea containing 20 mM DTT, 30 mM glycine, pH 10.0 required vigorous stirring for over 2 h at room temperature. All other steps were performed as described.[30] All samples were prepared under inert atmosphere inside a N_2-purged wet box. apoIPNS was exchanged into deuterated MOPS buffer (100 mM, pD = 7.4) and concentrated to 3−4 mM using a 10 kDa centricon tube. The sample was transferred to a sealed conical vial and made anaerobic by purging under an Ar atmosphere on a Schlenk line at 0 °C for approximately 1 h. Buffer was sealed in a conical vial and degassed by bubbling Ar through the solution on a Schlenk line. The Fe^{II}−IPNS complex was generated by microliter addition of an Fe^{II} stock solution prepared by dissolving Fe-$(NH_4)_2(SO_4)_2$ in degassed MOPS buffer (100 mM) to the apoIPNS. The Fe^{II}−IPNS−ACV complex was prepared through addition of a stock solution of ACV to the Fe^{II}−IPNS complex. ACV in degassed MOPS buffer (1 mM) was slowly added to the Fe^{II}−IPNS in microliter quantities with vigorous stirring between aliquots. NO was added to the Fe−IPNS−ACV complex by stirring the Fe−IPNS−ACV solution under an NO atmosphere for approximately 2−3 min. Glycerol-d_3 (60% (v/v), degassed by freeze/pump/thaw/heat) was added to the MCD and Abs samples as a glassing agent. CD spectra were collected with and without glycerol to ensure that the site was not affected by the addition of the glassing agent. EPR samples were prepared by diluting the Fe−IPNS−ACV−NO solution with degassed buffer (100 mM) to a concentration of approximately 100−150 μM.

2.3. Spectroscopic Methods. Near-IR (600−2000 nm) CD and MCD data were recorded on a Jasco J-200D spectropolarimeter with a liquid N_2-cooled InSb detector coupled to an Oxford Instruments SM4000-7T (T) superconducting magnet. UV/vis (300−900 nm) CD and MCD data were recorded on a Jasco J810 spectropolarimeter with an extended S-20 photomultiplier tube and adapter to accept an Oxford Instruments SM4000-7T superconducting magnet. MCD spectra were corrected for the natural CD and zero-field baseline effects by subtracting the 0T spectra at each temperature. VTVH-MCD data were collected using a calibrated Cernox resistor (Lakeshore Cryogenics, calibrated 1.5−300 K) inserted into the sample cell to accurately measure the sample temperature. VTVH data were normalized to the maximum observed intensity over all isotherms for a given wavelength, and the ground-state parameters were extracted by fitting utilizing published procedures. X-band EPR spectra were collected on a Bruker EMX spectrometer with Bruker ER 041XG/ER microwave bridges and ER 4102ST/ER 5106QT cavitities. Spectra were collected at temperatures between 8 and 50 K using an Oxford ITC503 temperature controller with an ESR 900 continuous flow cryostat.

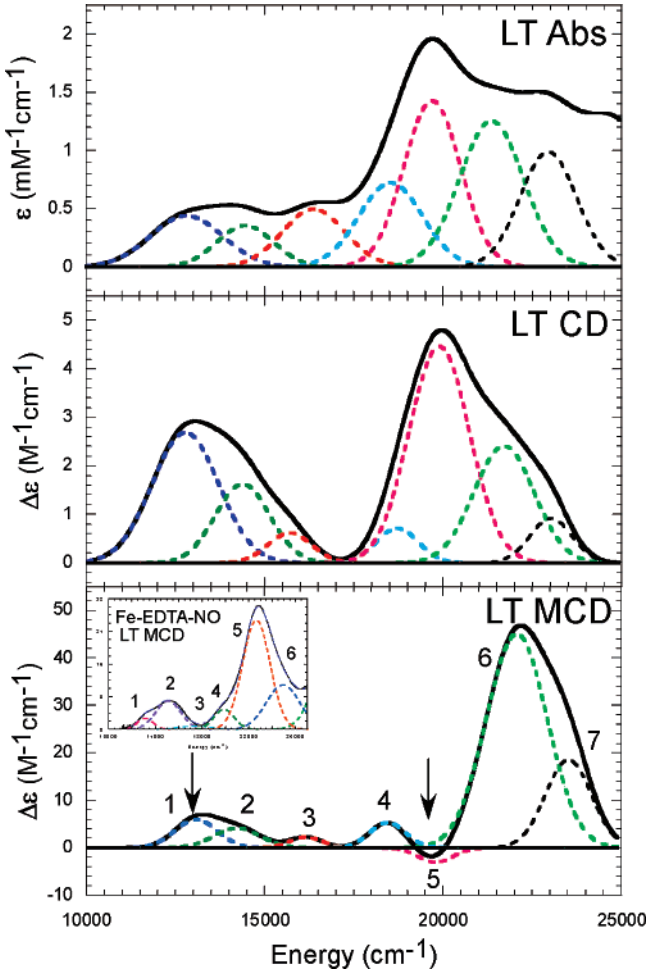

Figure 2. Absorbance (10 K, top), CD (5 K, middle) and MCD (5 K, 7 T, bottom) spectra collected for Fe−IPNS−ACV−NO with Gaussian best fits. Comparison to the MCD spectrum of Fe−EDTA−NO (inset) reveals two new spectral features seen in the spectra upon addition of ACV to Fe−IPNS−NO (arrows).

2.4. Computational Methods. The starting geometry for the Fe−IPNS−ACV−NO complex was taken from the crystal structure of Fe−IPNS−ACV−NO from *Aspergillus nidulans*.[17] Protein-derived ligands were truncated with imidizoles modeling histidines and propionate modeling aspartate. The ACV substrate was truncated to remove the six-carbon aminoadipoyl chain but was otherwise left intact. The alpha-carbons of the protein ligands were frozen relative to each other to impose the constraints of the protein backbone. The cysteine nitrogen and the two valine carboxylate oxygens of ACV were frozen relative to each other, and the alpha-carbons of the protein ligands to mimic

(29) Samson, S. M.; Belagaje, R.; Blankenship, D. T.; Chapman, J. L.; Perry, D.; Skatrud, P. L.; VanFrank, R. M.; Abraham, E. P.; Baldwin, J. E.; Queener, S. W.; Ingolia, T. D. *Nature (London)* **1985**, *318*, 191−194.
(30) Kriauciunas, A.; Frolik, C. A.; Hassell, T. C.; Skatrud, P. L.; Johnson, M. G.; Holbrook, N. L.; Chen, V. J. *J. Biol. Chem.* **1991**, *266*, 11779−11788.

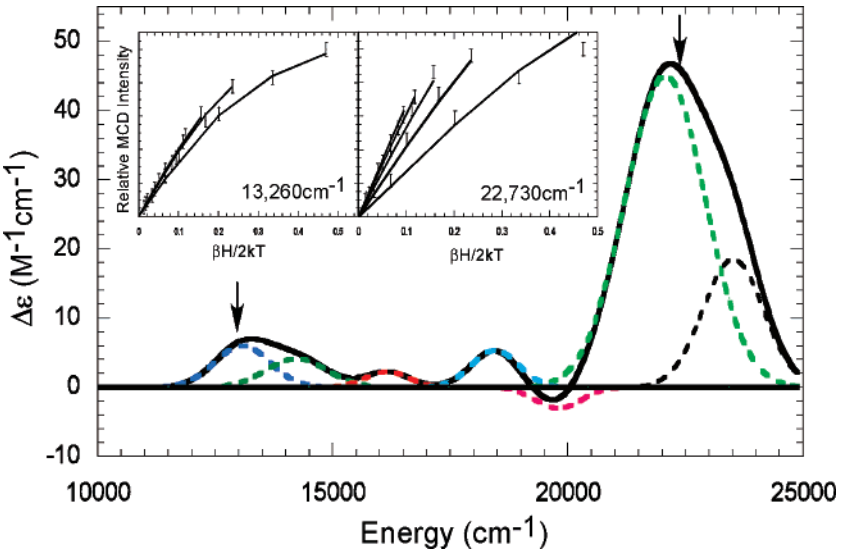

Figure 3. Fe−IPNS−ACV−NO VTVH MCD data collected at 13 260 cm^{-1} (left) and 22 730 cm^{-1} (right) demonstrate different nesting behaviors. (Arrows indicate energy where the isotherms were collected.)

hydrogen bonding to the substrate in the protein pocket. For the Fe−IPNS−ACV and Fe−IPNS−ACV−O_2 complexes, the starting geometry was taken from the optimized Fe−IPNS−ACV−NO complex with the NO moiety either removed or replaced with O_2 and optimized under the same conditions.

All complexes were geometry optimized using the Gaussian 03 software package,[31] with the spin unrestricted BP86 functional[32,33] with 10% Hartree−Fock exchange under tight convergence criteria. This functional was previously calibrated for {FeNO}^{7} complexes.[28] Geometry optimizations were carried out using the Pople 6-311G* basis set on Fe, S, and the NO/O_2 unit with the 6-31G* basis set on the remaining atoms. Single-point calculations were performed on the optimized structures to generate molecular orbitals using the functional and basis set above. Molecular orbital compositions were calculated using AOMix,[34,35] and optimized structures and molecular orbitals were visualized using Molden version 4.1.[36] Frequencies and thermodynamic parameters were calculated using the split 6-311G*/6-31G* basis set, and all frequencies were found to be real. In order determine the effects of the ACV thiolate on the energetics of NO and O_2 binding to Fe−IPNS−ACV, single-point energies were calculated for the Fe−IPNS−ACV 5C Fe^{II}, NO, and O_2 complexes using the 6-311+G(2d,p) basis set. Solvation effects to the energy of the optimized structure were included using the Polarized Continuum Model (PCM)[37] with a dielectric constant $\epsilon = 4.0$ to model the protein environment.

In order to correlate the calculated electronic structure of Fe−IPNS−ACV−NO to the spectroscopy, ΔSCF excitation energies were calculated with the Amsterdam Density Functional (ADF) package.[38−40] (The Gaussian package does not allow for ΔSCF calculations.) Using the Gaussian 03 optimized geometry, exited states were calculated for select charge-transfer transitions using the BP86 functional with the uncontracted triple-ξ basis set (TZP) with a single polarization function without any frozen core approximation. As ADF does not allow for the mixing of HF exchange for open-shell systems, the Zof Fe was set to 25.6 (single-point calculation) as was previously calibrated for similar calculations on {FeNO}^{7} model complexes.[28] All excitation energies were calculated by exciting a full electron to a virtual orbital except for the NO π^*(in-plane)→$Fe^{III}d_{xz}$ and S pseudo-σ →$Fe^{III}d_{z^2}$ transitions, which were calculated from Slater transitions because of convergence issues with the full electron excitation. Slater transitions were also evaluated for the transitions that converged in ΔSCF and gave the same results.

3. Results and Analysis

3.1. Spectroscopic Results. 3.1.1. Temperature-Dependent EPR. Previous EPR studies of Fe−IPNS−ACV−NO reported a signature $S = {}^3/_2$ spectrum with $g = 4.22$, 3.81, and 1.99 described by the spin Hamiltonian

$$\hat{H}_{\text{spin}} = D[S_z^2 - 5/4 + E/D(S_x^2 - S_y^2)] + g_0\beta\vec{S}\bullet\vec{H} \qquad (1)$$

where $g_0 = 2.0$ and D and E are the axial and rhombic Zero-Field Splitting parameters.[11] The E/D value was 0.035, indicative of a close to axial complex, with an increase in rhombicity upon binding of the substrate (the Fe−IPNS−NO complex had an $E/D = 0.015$). In order to obtain the value and sign of D, temperature-dependent EPR spectra of Fe−IPNS−ACV−NO were collected from 8 K to 50 K under nonsaturating conditions and the normalized intensity of the $g = 4.22$ signal was plotted versus temperature (Figure 1, insert). A Boltzmann fit to the Curie law dependence is given by eq 2

$$\text{Intensity} = \frac{C}{T}\left[\frac{1}{1 + \exp(-2D/kT)}\right] \qquad (2)$$

where C is the Curie constant, T is temperature in kelvin, and k is the Boltzmann constant. The best fit of the EPR intensity gives a value of $D = +12.5 \pm 0.5$ cm^{-1}. This is in good agreement with the magnitude of D previously obtained from Mössbauer spectroscopy of $D = 14 \pm 1$ cm^{-1}.[12]

3.1.2. Absorbance/CD/MCD Spectroscopy. Low temperature absorbance, CD, and MCD spectra were collected for the

(31) Frisch, M. J. et al. *Gaussian03*, revision C.03; Wallinford, CT, 2004 (http://www.gaussian.com).
(32) Becke, A. D. *Phys. Rev. A: At., Mol., Opt. Phys.* **1988**, *38*, 3098−3100.
(33) Perdew, J. P. *Phys. Rev. B. Condens. Mater.* **1986**, *33*, 8822−8824.
(34) Gorelsky, S. I. *AOMix program*, rev. 6.04. Available from: <http://www.sg-chem.net/>.
(35) Gorelsky, S. I.; Lever, A. B. P. *J. Organomet. Chem.* **2001**, *635*, 187−196.
(36) Schaftenaar, G.; Noordik, J. H. *J. Comput.-Aided Mol. Des.* **2000**, *14*, 123−134.
(37) Cramer, C. J.; Truhlar, D. G. *Chem. Rev.* **1999**, *99*, 2161−2200.
(38) te Velde, G.; Baerends, F. M. B. E. J.; Fonseca Guerra, C.; van Gisbergen, S. J. A.; Snijders, J. G.; Ziegler, T. *J. Comput. Chem.* **2001**, *22*, 931−967.
(39) Guerra, C. F.; Snijders, J. G.; Velde, G. t.; Baerends, E. J. *Theor. Chim. Acta* **1998**, *V99*, 391−403.
(40) ADF2004.01, SCM, Theoretical Chemistry, Vrije Universiteit, Amsterdam, The Netherlands, http://www.scm.com.

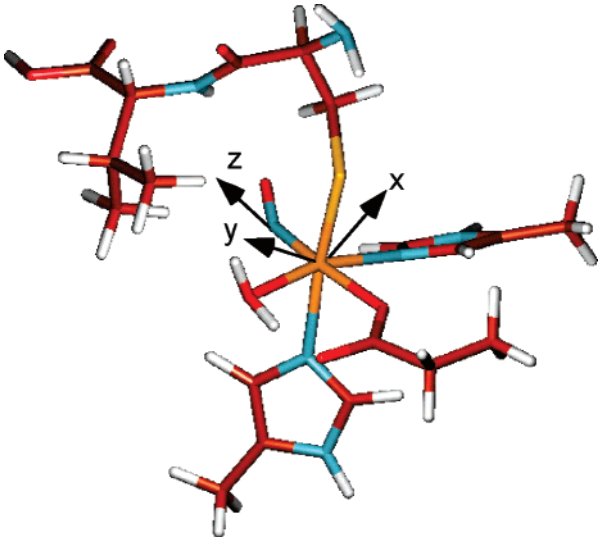

Figure 4. UBP86+10%HF/6-311G*/6-31G* optimized Fe−IPNS−ACV−NO complex.

Fe−IPNS−ACV−NO complex, and simultaneous Gaussian fitting of the spectra requires the presence of at least seven bands (Figure 2). Previous spectroscopic studies of {FeNO}^{7}model complexes report a signature pattern of five transitions in the Abs/MCD spectra of these complexes with two weak, low-energy features from Fe d → d ligand field (LF) transitions in the 11 000−15 000 cm^{-1} energy region, followed by three NO $2\pi^*$→Fe d charge transfer (CT) transitions in the 17 000−22 000 cm^{-1} energy region (insert, Figure 2 bottom).[27] Comparison of the Fe−IPNS−ACV−NO bands to those of the model complexes reveals two new features introduced by the addition of the ACV thiolate at approximately 13 100 cm^{-1} and 19 800 cm^{-1} (bands 1 and 5, indicated by arrows in MCD). The lower energy transition is the weaker of the two in intensity in all three spectra but is more intense than the Fe d→d LF transitions found in the same region of the spectra of the model complexes. There is a moderately intense absorbance feature coincident with band 1 seen in the room-temperature spectrum of Fe−IPNS−ACV−NO.[11] The transition at 19 800 cm^{-1} is very intense in low temperature absorbance and CD, dominating both spectra, but is weak and negative in the MCD spectrum (band 5). The low intensity of this negative MCD band is likely due at least in part to overlap with strong positive bands at lower and higher energy.

Variable temperature-variable field MCD (VTVH) data were collected on the Fe−IPNS−ACV−NO complex to determine the polarization of the bands at 13 100 cm^{-1} (band 1) and 22 100 cm^{-1} (band 6). Collection of VTVH data for band 5 was unsuccessful because of its low intensity and overlap with the bands to lower and higher energy. VTVH data collected at 13 260 and 22 730 cm^{-1} exhibit very different nesting behaviors and are consistent with these transitions having different polarizations (Figure 3, insert).[41]

MCD intensity is directly proportional to the spin-expectation values of the ground state sublevels, which can be generated from the spin-Hamiltonian. VTVH MCD data collected on a randomly oriented sample with $S \geq {}^1/_2$ can be modeled with eq 3

$$\frac{\Delta\epsilon}{E} = \frac{\gamma}{4\pi S}\int_0^{\pi}\int_0^{2\pi}\sum_i N_i(l_z\langle S_z\rangle_i M_{xy}^{\mathrm{eff}} + l_y\langle S_y\rangle_i M_{xz}^{\mathrm{eff}} + l_x\langle S_x\rangle_i M_{yz}^{\mathrm{eff}})\sin\theta\,\mathrm{d}\theta\,\mathrm{d}\phi \quad (3)$$

where x, y, and z refer to the principal axes of the ZFS tensor; N_i is the temperature-dependent Boltzmann population; l_x, l_y, and l_z are the direction cosines for the magnetic field relative to the molecular coordinate system; $\langle \boldsymbol{S}_{x,y,z}\rangle_i$ are the spin expectation values for the ith ground state sublevel; M_{ij}^{eff} are the products of the polarizations of the electronic transitions; and γ is a collection of constants. Using the spin Hamiltonian parameters D, E/D, and g_0 obtained from the EPR data, the effective transition moments M_{ij}^{eff} can be obtained from fitting the data (Figure 3, insert) using eq 3.[42] These transition moments can then be used to calculate the percent polarization along the ZFS tensor axes using eq 4 with cyclic permutations of the indices for the other polarizations.

$$\%x = 100 \times \left[\frac{(M_{xy}^{\mathrm{eff}}\,M_{xz}^{\mathrm{eff}})^2}{(M_{xy}^{\mathrm{eff}}\,M_{xz}^{\mathrm{eff}})^2 + (M_{xy}^{\mathrm{eff}}\,M_{yz}^{\mathrm{eff}})^2 + (M_{yz}^{eff}\,M_{xz}^{\mathrm{eff}})^2}\right] \quad (4)$$

From the fit of the VTVH isotherms at 22 730 cm^{-1}, the 22 100 cm^{-1} transition is 96.9% z-polarized. As LMCT bands are polarized along the metal−ligand bond, a strongly z-polarized transition is consistent with a transition along the dominant Fe−N$_{NO}$ bond, and this band can be assigned as a NO π^* → Fe d CT transition. (The z-axis lies along the short Fe−N$_{NO}$ bond, with the x and y axes designated as lying between the equatorial ligand−Fe bonds with x in the Fe−N−O plane (Fe−NO ∠ = 150° *vide infra*) between the Fe−S and Fe−N$_{His}$ bonds.) The fit of the 13 260 cm^{-1} isotherms shows the band to be 49.7% z-polarized and 50.3% x−y-polarized (x and y cannot be distinguished in this close to axial ZFS system), indicating a transition with both NO$^-$ → Fe^{III} (z) and RS$^-$ → Fe^{III} (x,y) CT character.

3.2. Computational Results. 3.2.1. Geometry Optimization. DFT calculations were performed on Fe−IPNS−ACV−NO to determine the effects of the Fe−ACV thiolate bond on the geometric and electronic structure of the IPNS {FeNO}^{7} unit. The optimized Fe−IPNS−ACV−NO complex is a distorted octahedron with an Fe−S bond distance of 2.35 Å, an Fe−N$_{NO}$ bond distance of 1.74 Å, and an Fe−N−O bond angle of 150.3° (Figure 4). This Fe−N$_{NO}$ geometry is markedly different than that reported in the Fe−IPNS−ACV−NO crystal structure (Table 1),[17] which has an Fe−N$_{NO}$ bond distance of 2.13 Å

Table 1. Geometric Parameters for {FeNO}^{7} Unit of Fe−IPNS−ACV−NO and Related Model Complex

	Fe–IPNS–ACV–NO crystal structure	Fe–IPNS–ACV–NO EXAFS	Fe–IPNS–ACV–NO optimized structure[a]	Fe–[Me$_3$TACN]–(N$_3$)$_2$–NO optimized structure[a]
Fe−N$_{NO}$	2.13 Å	1.71 Å	1.74 Å	1.72 Å
N−O	1.15 Å	N/A	1.19 Å	1.17 Å
Fe−N−O	119.7°	N/A	151°	148°

[a] UBP86+10%HF/6-311G*/6-31G* optimized structures.

(41) Due to the temperature instability of the Fe−IPNS−ACV−NO glass, VTVH data points were obtained from full MCD spectra collected at different temperatures and fields. This resulted in fewer data points and larger errors than normal for the VTVH data due to a temperature-dependent CD background.

(42) Neese, F.; Solomon, E. I. *Inorg. Chem.* **1999**, *38*, 1847−1865.

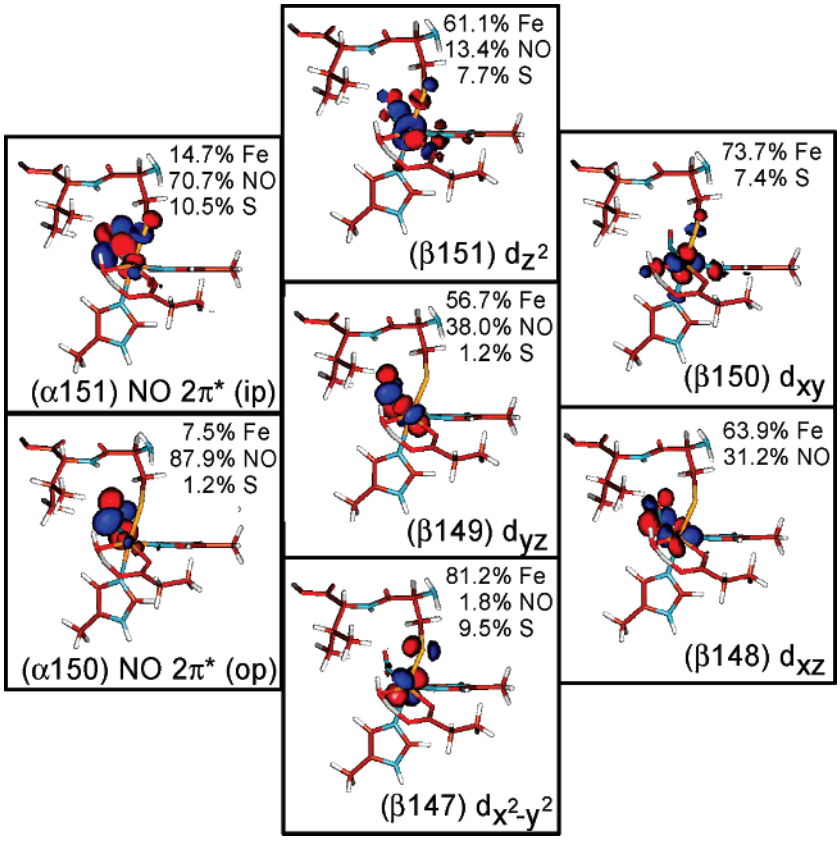

Figure 5. Contours of the lowest unoccupied α and β molecular orbitals from the ground state wavefunction of Fe−IPNS−ACV−NO.

with an Fe−N−O bond angle of 119.7°. However, the optimized Fe−N_{NO} geometry is in good agreement with the experimental Fe−N_{NO} bond distance determined by EXAFS which has an accuracy of ±0.02 Å[13] and with the Fe−N_{NO} bond distance and Fe−N−O bond angle previously determined for the {FeNO}^{7} model complex Fe−[Me_3TACN]−$(N_3)_2$−NO.[28] The Fe−S bond distance in the optimized Fe−IPNS−ACV−NO is consistent with an Fe^{III}−thiolate S bond. From the comparison to the model complex without thiolate ligation, the presence of the ACV thiolate does not significantly affect the geometry of the {FeNO}^{7} unit in the Fe−IPNS−ACV−NO complex.

3.2.2. Electronic Structure. Experimental and computational studies of the {FeNO}^{7} model complexes Fe−EDTA−NO and Fe−[Me_3TACN]−$(N_3)_2$−NO have determined the electronic structure of the {FeNO}^{7} unit to be a high-spin Fe^{III} ($S = {}^5/_2$) antiferromagnetically coupled to NO^- ($S = 1$).[27,28] The ground state wave function of this complex is best described by five unoccupied β Fe d molecular orbitals (MOs) and two unoccupied α NO 2π* MOs, with one NO π* MO located in the Fe−N−O plane (in-plane) and the other perpendicular to the Fe−N−O plane (out-of-plane). These unoccupied molecular orbitals are used to describe the bonding as they reflect the uncompensated occupied counterparts which give the major contribution to bonding. The MOs and energy level diagram for the optimized Fe−IPNS−ACV−NO complex are given in Figures 5 and 6, respectively. As seen in the model complexes, the two lowest unoccupied α MOs of Fe−IPNS−ACV−NO have mostly NO 2π* in-plane (ip) and out-of-plane (op) character, respectively, with small contributions from the Fe d orbitals and the ACV thiolate. In the β manifold, the five lowest unoccupied MOs are comprised mostly of Fe d character, with some contribution from the NO π* and ACV thiolate orbitals. (The corresponding occupied α Fe d MOs are stabilized by approximately 6 eV by spin polarization.) In the optimized Fe−IPNS−ACV−NO complex the spin densities on the Fe and NO are 3.44 and −0.79, respectively, which is consistent with the values calculated for the Fe−[Me_3TACN]−$(N_3)_2$−NO model complex.[28]

A previous density functional study of Fe−IPNS−ACV−NO described the electronic structure of the complex as high-spin Fe^{II} ($S = 2$) antiferromagnetically coupled to $NO^\bullet$ ($S = {}^1/_2$) based upon calculated spin densities and Mössbauer parameters.[26] While the calculated Fe−N_{NO} bond length used to calibrate the optimized structure by Zhang et al. (1.83 Å) is shorter than that reported in the crystal structure, it is longer than the experimental value obtained by EXAFS[13] and the calculated values of the {FeNO}^{7} model complexes[28] and the geometry optimized structure obtained here. A combination of MCD, resonance Raman, and XAS analysis has shown the model is a high-spin Fe^{III} ($S = {}^5/_2$) antiferromagnetically coupled to NO^- ($S = {}^1/_2$).[27] As the {FeNO}^{7} unit contains a very covalent Fe−NO bond, the Mössbauer parameters for {FeNO}^{7} complexes generally lie between those reported for high-spin octahedral Fe^{II} and Fe^{III}; however, Mössbauer studies of a series of {FeNO}$^{6-8}$ model complexes also concluded that the Fe center in {FeNO}^{7} is best described as a high-spin Fe^{III}.[43] Based on the better agreement with experimental geometric parameters, consistency with model complexes, and the occupancy of the MO orbitals, the electron structure of the Fe−IPNS−ACV−

(43) Hauser, C.; Glaser, T.; Bill, E.; Weyhermuller, T.; Wieghardt, K. *J. Am. Chem. Soc.* **2000**, *122*, 4352−4365.

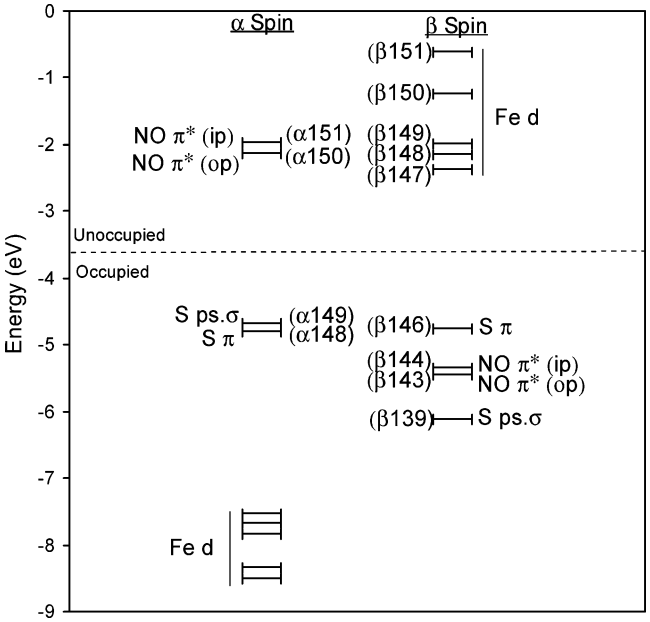

Figure 6. Molecular orbital diagram of Fe−IPNS−ACV−NO. The five lowest unoccupied β orbitals are comprised of mostly Fe d character, while the two lowest unoccupied α orbitals are comprised of mostly NOπ* character, consistent with an electronic structure description of a high-spin Fe^{III} antiferromagnetically coupled to NO$^-$.

NO complex is best described as a high-spin Fe^{III} ($S = {}^5/_2$) antiferromagnetically coupled to NO$^-$ ($S = 1$).

In addition to the Fe−NO bonding description, the MO and energy diagrams for Fe−IPNS−ACV−NO describe the interactions of the Fe^{III} and the ACV thiolate. The Fe-bound thiolate has two 3p orbitals (the third is tied up in the C−S bond) that can interact with the Fe^{III} d orbitals in either a pseudo-σ or π orientation.[44] From the Fe−IPNS−ACV−NO ground state wave function, the ACV thiolate lone pairs have a π interaction with $d_{x^2-y^2}$ orbital (Figure 5, contour β147, axes defined in Figure 4) and a pseudo-σ interaction with the d_{z^2} and d_{xy} orbitals (Figure 5, contours β151 and β150). These same interactions are also reflected in the α manifold, with the thiolate pseudo-σ interacting with the d_{z^2} orbital, which also interacts with the unoccupied NO π*(ip) orbital (Figure 5, contour α151). This MO has 10.5% S character, compared to 1.2% S character in the NO π*(op) orbital (Figure 5, contour α150), demonstrating a significant configuration interaction between the thiolate pseudo-σ and NO π*(ip) MOs mediated by the Fe d_{z^2} orbital. This configuration interaction raises the NO π*(ip) MO in energy (Figure 6) and reverses the order of the NO π* orbitals relative to that of the model complexes.

3.3. Spectral Assignment. 3.3.1. MCD Analysis. {FeNO}^{7} complexes demonstrate signature Absorbance/CD/MCD spectra with a common pattern of five transitions.[27] The first two are d → d ligand field (LF) transitions, which are spin forbidden but gain intensity through exchange coupling to the Fe^{III}, followed by three charge transfer (CT) transitions: NOπ*(in-plane) → Fe$^{III}d_{x^2-y^2}$, NO π*(in-plane) → Fe$^{III}d_{xz}$, and NO π*(out-of-plane) → Fe$^{III}d_{yz}$ with NO π*(out-of-plane) → Fe$^{III}d_{yz}$ being the most intense due to increased mixing of the NO π*(out-of-plane) and

(44) The π interaction results from overlap of the 3p orbital perpendicular to the Fe−S−C plane. The pseudo-σ interaction results from overlap in the plane, which is tilted off the Fe−S axes because the Fe−S−C angle is greater than 90°.

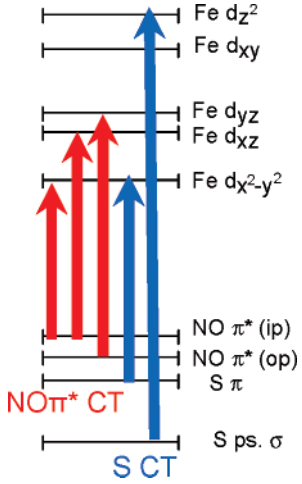

Figure 7. ΔSCF charge-transfer transition for the Fe−IPNS−ACV−NO complex calculated using ADF/BP86/TZV with $Z_{eff} = 25.6$.

Fe$^{III}d_{yz}$ orbitals. Comparison of the Fe−IPNS−ACV−NO MCD spectrum to that of the Fe−EDTA−NO model complex (Figure 2, insert) shows that bands 4 and 6 in the Fe−IPNS−ACV−NO spectrum correspond in both energy and relative intensity to bands 4 and 5 in the Fe−EDTA−NO spectrum, which are assigned as the NO π*(in-plane) → Fe$^{III}d_{xz}$ and NO π*(out-of-plane) → Fe$^{III}d_{yz}$ transitions in the Fe−EDTA−NO complex. Bands 2 and 3 in the IPNS spectrum correspond well with the weak d → d ligand field (LF) transitions (bands 1 and 2) in the Fe−EDTA−NO spectrum. Band 3 in the Fe−EDTA−NO spectrum is very weak and is located in an energy region that is overlapped in the Fe−IPNS−ACV−NO spectrum by the presence of band 5. Bands 1 and 5 have no counterpart in the Fe−EDTA−NO spectrum and are therefore new features induced by the binding of the ACV thiolate.

From the ACV thiolate interaction with Fe^{III} in the Fe−IPNS−ACV−NO complex one would expect two additional transitions: (1) a S π to Fe $d_{x^2-y^2}$ CT transition and (2) a S pseudo-σ to Fe d_{z^2} CT transition, with the S π to Fe d CT transition significantly lower in energy. While the new bands 1 and 5 potentially match the number of anticipated for thiolate CT, the rules governing MCD intensity can be used to rigorously assign the new transitions. The MCD spectrum of Fe−IPNS−ACV−NO possesses a unique feature in that the transition at 19 800 cm^{-1} has negative intensity, creating a pattern of alternating positive and negative intensity referred to as a Pseudo-A Term, which has certain electronic structure requirements in order to occur in the MCD spectrum.[42] First, the complex must have two spin−orbit coupled (SOC) excited states with perpendicular transition dipole moments. These two charge-transfer excited states must only differ by one electron on a single center, so they must share either a common donor or acceptor orbital. Finally, the orbitals which differ by one electron must rotate into each other by spin−orbit coupling L_i in a direction i perpendicular to the two transition moments.

In the Fe−IPNS−ACV−NO complex, the ACV thiolate S is bound *cis* to the NO, so any thiolate S → Fe d CT and NO → Fe d CT transitions will have perpendicular transition dipole moments. Using the Kohn−Sham ground state orbitals from the DFT calculations (Figure 6), the electron configurations of the S pseudo-σ → Fe d and S π → Fe d CT excited states can be compared to those of the NO π* → Fe d CT excited states

Table 2. Calculated ΔSCF/ADF and Experimental Energies of CT Transitions in {FeNO}^{7} Complexes

transition	Fe–[Me_3TACN]–NO experiment (cm^{-1})	Fe–[Me_3TACN]–NO ΔSCF/ADF	IPNS–ACV–NO experiment	IPNS–ACV–NO ΔSCF/ADF
NO π^*(ip) → $d_{x^2-y^2}$	17 400	15 975	13 100	13 280
NO π^*(ip) → d_{xz}	19 650	19 565	18 500	17 420
NO π^*(op) → d_{yz}	22 580	19 950	22 100	21 320
S π → $d_{x^2-y^2}$	N/A	N/A	19 800	22 980
S ps.σ → d_{z^2}	N/A	N/A		30 600

to look for transitions with the same acceptor orbital. (The donor orbitals are different.) The acceptor orbital for the S pseudo-σ transition is the Fe d_{z^2} orbital; however, no NO π^* → Fe d CT transitions excite an electron into that orbital. Therefore no SO mechanism exists to couple the S pseudo-σ → Fe d_{z^2} transition with the NO π^* → Fe d CT transitions. The other possible assignment of band 5 is the S π → Fe $d_{x^2-y^2}$ CT transition. As the two excited states associated with the S π → Fe $d_{x^2-y^2}$ CT transition and the NO π^* (ip) → Fe $d_{x^2-y^2}$ CT transitions both excite an electron into the Fe $d_{x^2-y^2}$ orbital, these excited states differ by one electron in donor orbitals, potentially creating a Pseudo-A term.

Strong covalent interactions mix $d_{x^2-y^2}$ and d_{xz} character into the S π and NO π^* (ip) donor orbitals, respectively, which allows the Fe-based SO operator to couple these two CT excited states. Because the LMCT transitions are polarized along the molecular axes of the complex, the *x* and *y* axes were rotated by 45° to be colinear with the Fe−ligand bonds (*x* along the Fe−S bond and *y* along the Fe−N_{His} bond). Using these newly defined axes, the Fe components of the donor orbitals are transformed from $d_{x^2-y^2}$ to $d_{x'y'}$ and from d_{xz} to $d_{x'z'} + d_{y'z'}$.

In order to create a pseudo A-term, the two orthogonal LMCT transitions must SOC in the third orthogonal direction. The S π → Fe $d_{x^2-y^2}$ CT transition occurs in the *x*′ direction, and the NO π^* (ip) → Fe $d_{x^2-y^2}$ CT transition occurs in the *z*′ direction. Because $L_{y'}$ rotates $d_{x'y'}$ into $d_{y'z'}$, the S π → Fe d CT transition and the NO π^* (ip) → Fe d CT transition will couple to produce a pseudo A-Term feature in the Fe−IPNS−ACV−NO MCD spectrum. From this MCD intensity analysis, the negative band at 19 800 cm^{-1} is assigned as the S π → Fe $d_{x^2-y^2}$ CT transition.

3.3.2. ΔSCF Calculations. In order to confirm the assignment of band 5 as the S π → Fe $d_{x^2-y^2}$ CT transition and to identify the source of the low-energy band 1 introduced by binding the ACV thiolate ligand, ΔSCF calculations were performed for the NO π^* → Fe d and S → Fe d CT transitions (Figure 7). Using the Kohn−Sham ground state generated from the optimized Fe−IPNS−ACV−NO complex, the energies of five CT transitions were calculated: NOπ^*(in-plane) → $Fe^{III}d_{x^2-y^2}$, NO π^*(in-plane) → $Fe^{III}d_{xz}$, NO π^*(out-of-plane) → $Fe^{III}d_{yz}$, Sπ→$Fe^{III}d_{x^2-y^2}$ and S pseudo-σ → $Fe^{III}d_{xy}$ and the calculated energies and their correlation to Fe−[Me_3TACN]−$(N_3)_2$−NO are given in Table 2.

The energy of Sπ→$Fe^{III}d_{x^2-y^2}$ CT transition is calculated to be 22 980 cm^{-1}, in reasonable agreement with the experimental energy of band 5 in the MCD spectrum, further confirming the MCD Pseudo A-Term assignment of this band. The S pseudo-σ → $Fe^{III}d_{xy}$ CT transition is calculated to be substantially higher in energy, as would be expected from the one electron orbital diagram, and this can be excluded as an assignment of either band 1 or band 5. It is interesting to note that from the Kohn−Sham ground state diagram the Sπ → $Fe^{III}d_{x^2-y^2}$ CT transition involves promotion from the β HOMO to LUMO and would be expected to be lower in energy than the NO π^* → Fe^{III}d CT transitions. However, the Sπ → $Fe^{III}d_{x^2-y^2}$ CT transition is calculated to be higher in energy than the NO π^*(ip) → $Fe^{III}d_{xz}$ transition and similar in energy to the NO π^*(op) → $Fe^{III}d_{yz}$ transition as observed experimentally. This reordering of transition energies from the ground state prediction results from the differences in orbital covalency of the donor/acceptor pairs for the Sπ → $Fe^{III}d_{x^2-y^2}$ and the NO π^*→Fe^{III}d CT transitions. The Sπ→$Fe^{III}d_{x^2-y^2}$ transition involves excitation of an electron from a donor largely centered on the S ligand to an acceptor largely centered on Fe, which increases the electron repulsion in the excited state. The donor and acceptor orbitals for the NO π^* → Fe^{III}d CT transitions are much more covalent, so the electron repulsion in their ground and excited states is similar. As a result of this difference in electron repulsion, the Sπ → $Fe^{III}d_{x^2-y^2}$ CT transition is shifted higher in energy than would be expected from the energy splitting in the one-electron Kohn−Sham ground state diagram.

From Table 2, the energy of the NOπ^*(in-plane) → $Fe^{III}d_{x^2-y^2}$ is calculated to be 13 280 cm^{-1}, in good agreement with the energy of band 1 in the MCD spectrum of Fe−IPNS−ACV−NO. The calculated energy for the NOπ^*(in-plane) → $Fe^{III}d_{x^2-y^2}$ is substantially lower than both the experimental and calculated energy for the same transition in Fe−[Me_3TACN]−$(N_3)_2$−NO. From the VTVH MCD data, band 1 is half *z*-polarized, which would correspond with a NOπ^* → Fe^{III} d CT transition, but the *x*,*y*-polarization which is also present would correspond to S character mixed into the transition. Examination of the donor and acceptor orbitals for the NOπ^*(in-plane) → $Fe^{III}d_{x^2-y^2}$ transition shows significant S character in both the NOπ^*(ip) and $Fe^{III}d_{x^2-y^2}$ orbitals (10.5% and 9.5% S, respectively, Figure 5, contours α151 and β147). This S character will mix *x*,*y*-polarized intensity into the NOπ^*(ip) → $Fe^{III}d_{x^2-y^2}$ CT transition and lead to the increased intensity in this band relative to the very weak NOπ^*(ip) → $Fe^{III}d_{x^2-y^2}$ CT band in the Fe−[Me_3-TACN]−$(N_3)_2$−NO spectra. Configuration interaction of the S pseudo-σ MO with the NOπ^*(ip) MO raises the energy of the donor orbital, lowering the transition in energy.

The two remaining NOπ^*(ip) → $Fe^{III}d_{xz}$ and NO π^*(op) → $Fe^{III}d_{yz}$ transitions were calculated at similar energies to the experimental and calculated values of the same transitions in the Fe−[Me_3TACN]−$(N_3)_2$−NO model complex. It is interesting to note that while the NOπ^*(ip) → $Fe^{III}d_{x^2-y^2}$ and NOπ^*-(ip) → $Fe^{III}d_{xz}$ transitions share the same donor orbital, only the NOπ^*(ip) → $Fe^{III}d_{x^2-y^2}$ transition is shifted to significantly lower energy. The $Fe^{III}d_{xz}$ acceptor orbital has more antibonding ligand character than the $Fe^{III}d_{x^2-y^2}$ orbital, shifting it to higher energy. Thus while configuration interaction shifts the donor orbital up in energy, the acceptor orbital for the NOπ^*(in-plane) → $Fe^{III}d_{xz}$ transition is also shifted up in energy and the transition energy is not greatly changed relative to the model complex.

Table 3. Geometric Parameters for {FeO$_2$}^{8} Unit of Fe−IPNS−ACV−O$_2$ and Related Model Complex

geometric parameter	Fe–IPNS–ACV–O$_2$ optimized complex	Fe–[Me$_3$TACN]–O$_2$–(N$_3$)$_2$ optimized complex
Fe−O	1.87 Å	1.88 Å
O−O	1.31 Å	1.29 Å
Fe−S	2.33 Å	N/A
Fe−O−O	134°	130°

3.4. {FeNO}^{7} → {FeO$_2$}^{8}. 3.4.1. Geometry Optimization of Fe−IPNS−ACV−O$_2$. In order to explore the reaction coordinate of Fe−IPNS−ACV with O$_2$, the NO moiety of the Fe−IPNS−ACV−NO complex was replaced with O$_2$ in the crystal structure geometry and the complex was optimized. As O$_2$ could theoretically bind to Fe−IPNS−ACV to give complexes of $S = 1$, 2, or 3, the complex was optimized in each of the three spin states with the $S = 2$ complex lower in energy than the $S = 1$ and $S = 3$ complexes by 2.2 and 3.7 kcal/mol, respectively. Relevant geometric parameters for the optimized $S = 2$ Fe−IPNS−ACV−O$_2$ complex and the optimized Fe−[Me$_3$TACN]−(N$_3$)$_2$−O$_2$ complex[28] are given in Table 3. Comparison of the Fe−O and O−O bond distances and the Fe−O−O bond angle in the two complexes reveal similar Fe−O$_2$ geometries (Table 3). The Fe−S bond distance is relatively unchanged by the replacement of NO with O$_2$ (2.33 versus 2.35 Å).

3.4.2. Electronic Structure of Fe−IPNS−ACV−O$_2$. Previous calculations on the Fe−[Me$_3$TACN]−(N$_3$)$_2$−O$_2$ complex describe an electronic structure of a high-spin Fe^{III} antiferromagnetically paired to O$_2^{\bullet-}$ superoxide to give an $S = 2$ complex.[28] O$_2$ has one more electron than NO, so when it bonds to Fe^{II} this extra electron fills one of the unoccupied π^* orbitals relative to the {FeNO}^{7}. The ground state wave function of the Fe^{III}−superoxide complex is characterized by five unoccupied β Fe d MOs and one unoccupied α O$_2$ π^* MO. The MOs and the energy level diagram for the optimized Fe−IPNS−ACV−O$_2$ complex are given in Figures 8 and 9, respectively. As found in the Fe−[Me$_3$TACN]−(N$_3$)$_2$−O$_2$ complex, the two lowest unoccupied β MOs of Fe−IPNS−ACV−O$_2$ have mostly Fe d character, with some contribution from the O$_2$ π^* and ACV thiolate orbitals. In the α manifold, the lowest unoccupied MO contains mostly O$_2$ 2π^* in-plane (ip) character with additional small contributions from the Fe d orbitals and the ACV thiolate. In the optimized Fe−IPNS−ACV−O$_2$ complex the spin densities on the Fe and O$_2$ are 3.79 and −0.22, respectively, which is consistent with the values calculated for the Fe−[Me$_3$TACN]−(N$_3$)$_2$−O$_2$ model complex.

However, the electronic structure of the Fe−IPNS−ACV-O$_2$ complex differs from that of the model complex in one important aspect. In the Fe−[Me$_3$TACN]−(N$_3$)$_2$−O$_2$ complex, the lowest unoccupied α MO is the O$_2$ π^* (op) orbital, while, in the IPNS complex, the lowest unoccupied α MO is the O$_2$ π^* (ip) orbital (Figure 8, contour α151). From the electronic structure of the Fe−IPNS−ACV−NO complex, there is a configuration interaction between the thiolate S pseudo-σ and the NOπ^* (ip) orbital, which raises the π^* (ip) orbital in energy. When an extra electron is added in going from the {FeNO}^{7} to {FeO$_2$}^{8} complex, this electron occupies the lower energy O$_2$ π^* (op) orbital. The occupation of the O$_2$ π^* (op) has direct mechanistic implications that are examined in the Discussion.

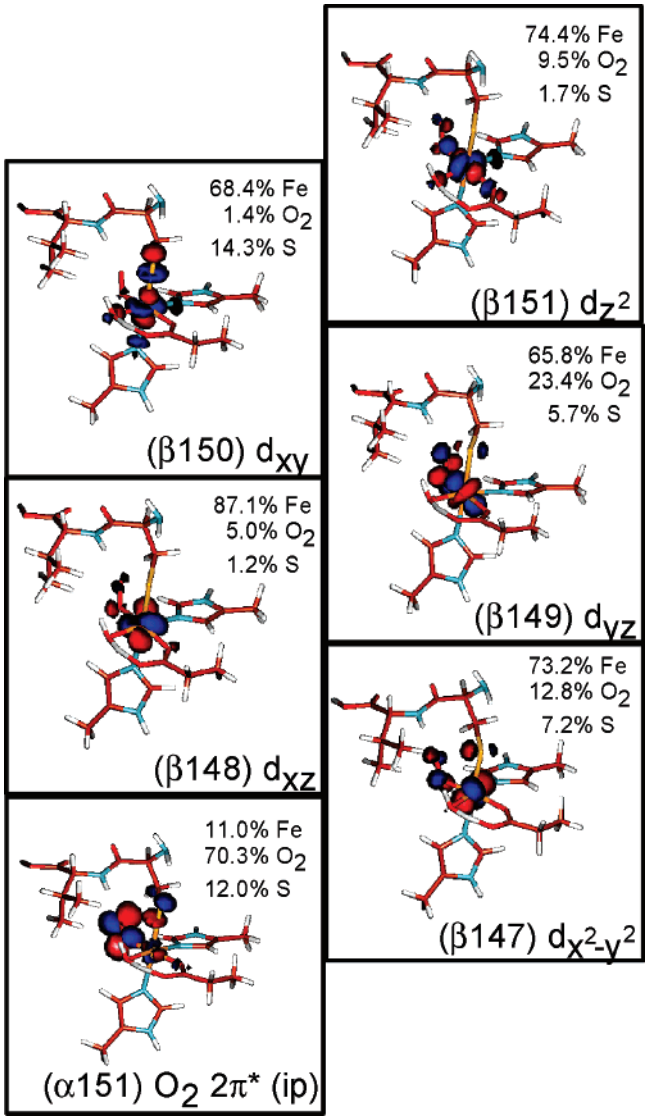

Figure 8. Contours of the lowest unoccupied α and β molecular orbitals from the ground state wavefunction of Fe−IPNS−ACV−O$_2$.

3.4.3. Energetics of NO/O$_2$ Binding to Fe−IPNS−ACV: Comparison to Non-Thiolate Liganded Nonheme Fe. While the electronic structure of the Fe−IPNS−ACV−O$_2$ is best described as a high-spin Fe^{III}−superoxide complex, the energetics of the formation of this complex must be explored to better understand the enzyme reaction mechanism. Previous studies of the energetics of NO and O$_2$ binding to the Fe−[Me$_3$TACN]−(N$_3$)$_2$−O$_2$ determined that the binding of NO to nonheme Fe^{II} is highly exergonic (∼ −20 kcal/mol) compared to O$_2$ binding, which is thermoneutral in the model complex.[28] In order to determine the source of the different binding energies of NO/O$_2$, the reaction was separated into the transfer of an electron from Fe^{II} to NO/O$_2$ to give Fe^{III} and NO$^-$/O$_2^{\bullet-}$ at infinite distance and the subsequent formation of the Fe^{III}−NO$^-$/O$_2^{\bullet-}$ bond. The transfer of the electron to NO/O$_2$ is highly endergonic, with the reduction of O$_2$ approximately 5 kcal/mol more favorable than that of NO. However the Fe^{III}-NO$^-$ bond formed is much stronger than the Fe^{III}-O$_2^{\bullet-}$ bond, providing the driving force for the reaction. In the mononuclear nonheme Fe enzyme DHBD, the binding of O$_2$ is calculated to be even less favorable than that in the model complex, with a highly endergonic energy

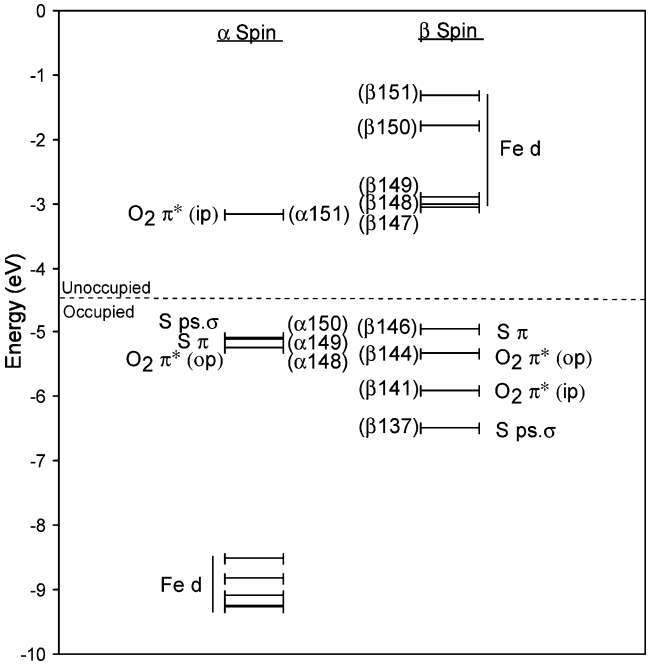

Figure 9. Molecular orbital diagram of Fe−IPNS−ACV−O_2. The five lowest unoccupied β orbitals are comprised of mostly Fe d character, while the lowest unoccupied α orbital is comprised of mostly O_2 π^* character, consistent with an electronic structure description of a high-spin Fe^{III} antiferromagnetically coupled to $O_2^{\bullet-}$.

of formation for the $Fe^{III}-O_2^{\bullet-}$ complex ($\Delta G \geq +20$ kcal/mol).[45] Thus nonheme Fe^{II} complexes are reasonably stable in O_2 in the absence of a redox active cofactor or substrate to supply additional electrons for the favorable two-electron reduction of O_2.

In order to estimate the influence of the ACV thiolate coordination on the binding of NO and O_2 to Fe−IPNS−ACV, calculations were performed comparing the NO/O_2 binding energy of Fe−IPNS−ACV to a non-thiolate liganded mononuclear nonheme Fe site. The crystal structure of the resting form of phenylalanine hydroxylase (PAH)[46] was used as a starting structure for Fe^{II} coordinated by the facial triad of two histidines and one monodentate aspartate, with two waters filling the remaining coordination positions in the five-coordinate (5C) resting complex. The 5C Fe^{II} structures of IPNS−ACV and PAH were optimized using UBP86+10%HF/6-311G*/6-31G*, and subsequently an electron was removed and the 5C Fe^{III} complexes were optimized. Finally, the PAH−NO and PAH−O_2 complexes were optimized for comparison with the Fe−IPNS−ACV−NO and O_2 complexes. In order to properly account for the diffuse nature of the S atom of the ACV thiolate and to avoid any basis set superposition error that may be introduced in calculating the formation energy of a bimolecular reaction, the energy of each species was calculated using the 6-311+G(2d,p) basis set with the PCM solvent model ($\epsilon = 4.0$). The energy profiles for NO/O_2 binding to Fe−IPNS−ACV and Fe−PAH are given in Figure 10.

As with the model complex and previous DHDB enzyme calculations,[28,45] the binding of NO to Fe−PAH is exergonic

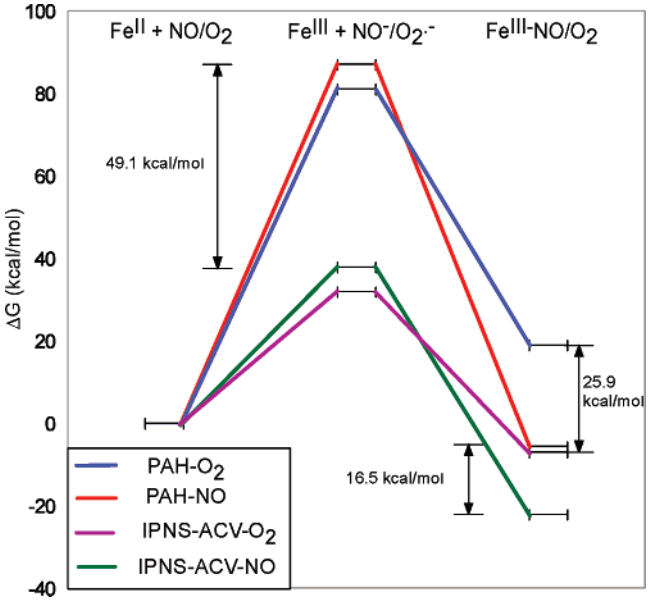

Figure 10. Energy profiles of NO/O_2 binding to Fe−IPNS−ACV and Fe−PAH.

($\Delta G = -5.7$ kcal/mol) while the binding of O_2 to Fe−PAH is highly endergonic ($\Delta G = 18.9$ kcal/mol). In the Fe−IPNS−ACV complex, the binding of NO is stabilized relative to Fe−PAH−NO and is much more exergonic ($\Delta G = -22.2$ kcal/mol). Importantly, the binding of O_2 to Fe−IPNS−ACV has also been stabilized relative to Fe−PAH−O_2, to the extent that the formation of Fe−IPNS−ACV−O_2 is exergonic ($\Delta G = -7.0$ kcal/mol). Examination of the energy profile shows that the Fe^{III} complex is stabilized by 49.1 kcal/mol in Fe−IPNS−ACV relative to Fe−PAH, which corresponds to a 2.1 eV stabilization in the oxidation of Fe^{II} to Fe^{III} in the presence of the ACV thiolate ligand. The Fe−S bond length decreases from 2.40 to 2.24 Å upon oxidation of the Fe^{II} to Fe^{III}, indicative of greater thiolate donation to the Fe upon oxidation. Also, the charge on the Fe in the ferric IPNS−ACV complex is 1.45, compared with 1.67 in the ferric PAH complex, again showing donation of a negative charge from the ACV thiolate to stabilize the positive charge on the Fe^{III} and render the formation of the IPNS−ACV Fe^{III}−superoxide complex energetically favorable.

4. Discussion

We have used a combination of EPR, absorbance, CD, MCD, and VTVH-MCD spectroscopies in conjunction with DFT calculations to study the {FeNO}^{7} complex of Isopenicillin *N*-synthase bound with its substrate ACV. Comparison of the MCD spectrum of Fe−IPNS−ACV−NO to that of previously studied {FeNO}^{7} model complexes reveals two new spectroscopic features associated with the binding of the ACV thiolate to the {FeNO}^{7} unit of Fe−IPNS−ACV−NO at approximately 13 100 and 19 800 cm^{-1}, assigned as the NO π^*(ip) → Fe $d_{x^2-y^2}$ and S π→ Fe $d_{x^2-y^2}$ CT transitions, respectively. The calculated ground state wavefunction of the Fe−IPNS−ACV−NO complex and VTVH-MCD data collected on the 13 100 cm^{-1} band reveal a configuration interaction between the S pseudo-σ and NO π^*(ip) orbitals, which shifts the NO π^*(ip) → Fe $d_{x^2-y^2}$ transition to lower energy and increases its intensity relative to the {FeNO}^{7} model complexes. When we replace NO with O_2 in the Fe−IPNS−ACV complex, the optimized Fe−IPNS−

(45) Davis, M. I.; Wasinger, E. C.; Decker, A.; Pau, M. Y. M.; Vaillancourt, F. H.; Bolin, J. T.; Eltis, L. D.; Hedman, B.; Hodgson, K. O.; Solomon, E. I. *J. Am. Chem. Soc.* **2003**, *125*, 11214−11227.
(46) Andersen, O. A.; Flatmark, T.; Hough, E. *J. Mol. Biol.* **2001**, *314*, 279−291.

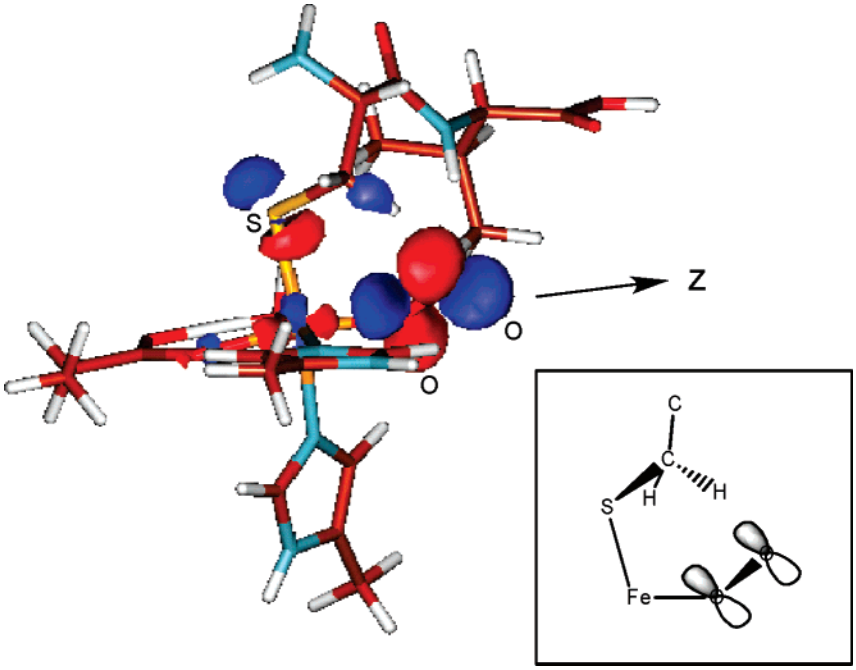

Figure 11. Fe−IPNS−ACV−O_2 FMO with proper orientation for H-atom abstraction of cysteine β-methylene H from ACV.

ACV−O_2 complex is best described as high-spin Fe^{III} antiferromagnetically coupled to superoxide, as is calculated for {FeO_2}^{8} model complexes. However, unlike the model complexes, the configuration interaction between the S pseudo-σ and O_2 π^*(ip) orbitals observed both computationally and spectroscopically in the Fe−IPNS−ACV−NO complex lifts the degeneracy of the π^* orbitals in the Fe−IPNS−ACV−O_2 complex. In going from {FeNO}^{7} to {FeO_2}^{8}, the extra electron occupies the lower energy O_2 π^*(op) orbital in the Fe−IPNS−ACV−O_2 complex, leaving the O_2 π^*(ip) unoccupied and available as a low lying Frontier Molecular Orbital (FMO).

This FMO has direct mechanistic implications in that the first proposed step in the reaction with substrate is the abstraction of the methylene H-atom from the cysteine β carbon;[17] therefore an unoccupied FMO with the proper orientation and character on the distal O must be available to overlap with the methylene H and accept an electron. The unoccupied O_2 π^* (ip) orbital in the Fe−IPNS−ACV−O_2 complex is oriented such that there is σ overlap with respect to the methylene H with high distal O character (Figure 11). The VTVH MCD data on Fe−IPNS−ACV−NO give direct experimental evidence for the mixing of S character into the NOπ^*(ip) → $Fe^{III}d_{x^2-y^2}$ CT transition. In the O_2 complex this configuration interaction of the S pseudo-σ and the O_2 π^* (ip) orbital insures this is the unoccupied FMO with proper orientation for H-atom abstraction.

In order to determine how the binding of the ACV thiolate affects the formation energies of the Fe−IPNS−ACV−NO and −O_2 complexes, we have calculated the energetics of NO/O_2 binding to the IPNS−ACV complex and to a non-thiolate liganded nonheme Fe complex modeled on phenylalanine hydroxylase.[46] In comparison to the PAH model, the ACV thiolate stabilizes NO binding to Fe−IPNS−ACV ($\Delta G = -22.2$ kcal/mol) and, importantly, stabilizes the energy of O_2 binding to Fe−IPNS−ACV to the extent that the formation of Fe−IPNS−ACV−O_2 becomes exergonic ($\Delta G = -7.0$ kcal/mol). By separating the oxidation of Fe^{II} and reduction of NO/O_2 from the subsequent $Fe^{III}-NO^-/O_2^{\bullet-}$ bond formation (Figure 10), we have determined that the charge donation from the ACV thiolate stabilizes the oxidation of Fe^{II} to Fe^{III}, allowing the IPNS−ACV complex to form a now energetically favorable Fe^{III}−superoxide complex. Through calculations, we have demonstrated the Fe^{III}−IPNS−ACV−superoxide complex is energetically accessible, and therefore a reasonable description of the IPNS mechanism is that it proceeds through H-atom abstraction by an Fe^{III}−superoxide species.

The thiolate stabilization of the Fe^{III}−IPNS−ACV−superoxide complex has major mechanistic implications for enzyme reactions. Many mononuclear nonheme Fe enzymes bind O_2 and activate it for reaction with an organic substrate; however, most of these enzymes overcome the unfavorable one-electron reduction of O_2 to superoxide by obtaining additional electron(s) from a redox active substrate or cofactor.[3] The additional electron is generally gained by O_2 binding in a bridging fashion to both the Fe center and the redox active cofactor or cosubstrate, as is proposed to occur in the αKG-dependent enzymes, pterin-dependent enzymes, and diol dioxygenases. Oxygen insertion occurs in the dioxygenases through this bridged binding of O_2 reduced to the peroxide level to both the Fe and either the substrate, as in the extradiol catechol dioxygenases, or the cosubstrate, as in the αKG- and pterin-dependent enzymes (Figure 12). With the stabilization gained by the charge donation of the ACV thiolate, IPNS can form an energetically favorable Fe^{III}−superoxide complex without having to bind O_2 in a bridging manner to gain the extra electron for peroxide formation. From our spectroscopic and DFT studies, this Fe only centered O_2 reactivity is directly controlled by the binding of the ACV thiolate to the Fe−IPNS−ACV complex. The binding of the ACV thiolate lowers the potential and drives the reaction at the Fe center, allowing for oxidase reactivity in IPNS without the oxygen atom insertion into the cosubstrate.

The formation of the IPNS−ACV Fe^{III}−superoxide complex is both energetically favorable and presents the correct FMO for H-atom abstraction from the Cysteine methylene C for the first step of the IPNS reaction with ACV. While one of the

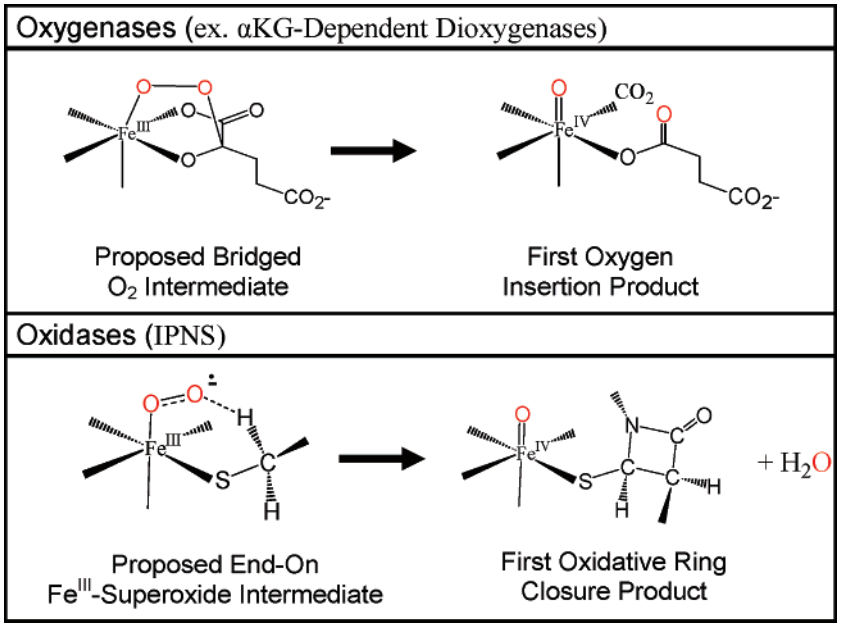

Figure 12. Comparison of plausible intermediates for mononuclear nonheme Fe oxygenases (αKG-dependent dioxygenases, shown top) and oxidases (IPNS, shown bottom).

proposed IPNS−ACV reaction mechanisms[17] calls for H-atom abstraction by an FeO_2 complex, this study presents the first experimental/computational evidence for the formation of an Fe^{III}−superoxide complex in IPNS. We are currently using this Fe−IPNS−ACV−O_2 model to further explore the reaction coordinate of IPNS and determine the influence of the ACV thiolate binding on later steps in the reaction mechanism.

Acknowledgment. This research was supported by NIH Grant GM40392 (E.I.S.) and NIH Grant GM24689 (J.D.L.). We thank Michael Mbughuni for assistance in preparation of IPNS.

Supporting Information Available: Cartesian coordinates of the geometry optimized model of the Fe−IPNS−ACV−NO active site complex with Gaussian BP86+10% Hartree−Fock (Table S1); Relevant structural parameters for the optimized Fe−IPNS−ACV−NO complex (Table S2); Cartesian coordinates of the geometry optimized model of the Fe−IPNS−ACV−O_2 active site complex with Gaussian BP86+10% Hartree−Fock (Table S3); Relevant structural parameters for the optimized Fe−IPNS−ACV−O_2 complex (Table S4); Cartesian coordinates of the geometry optimized models of the Fe−IPNS−ACV, Fe−PAH, Fe−PAH−NO, and Fe−PAH−O_2 active site complexes used to calculated NO/O_2 binding (Tables S5−S8); Complete ref 31. This material is available free of charge via the Internet at http://pubs.acs.org.

JA071364V